PHILOSOPHICAL TRANSACTIONS OF THE ROYAL SOCIETY A MATHEMATICAL, PHYSICAL & ENGINEERING SCIENCES

Photofragment Mapping of Intramolecular Motion [and Discussion]

M. Brouard, M. T. Martinez, J. O'Mahony, J. P. Simons and F. F. Crim

Phil. Trans. R. Soc. Lond. A 1990 **332**, 245-258
doi: 10.1098/rsta.1990.0112

Photofragment mapping of intramolecular motion

By M. Brouard, M. T. Martinez, J. O'Mahony and J. P. Simons
Chemistry Department, The University, Nottingham NG7 2RD, U.K.

The intramolecular motion in selected rovibrational levels in HOOH and HOOD, populated by tunable, pulsed laser excitation in the third O–H overtone band, has been probed via 'photofragment mapping' following secondary photon absorption. Quantum state distributions, vector correlations and vibrational (v_1, v_2) and rotational $(N_1\ \langle N_2 \rangle)$ OH(D) fragment pair correlations have been obtained using polarized, Doppler resolved laser induced fluorescence techniques. The results provide quantitative estimates of the extensive intramolecular redistribution of energy among the overtone levels and highlight the role of a-axis rotation in promoting rotation–vibration coupling.

1. Introduction

Photofragment mapping has a long history. It began with Neujmin & Terenin's (1934) classic discovery of very high rotational excitation in the OH(A) fragments generated in the vacuum ultraviolet photodissociation of water. This led to the realization, many years later, that the rotational excitation reflected a bent-through-linear parent molecular geometry change (Carrington 1964). The 'dynamical resonances' predicted to accompany the dissociation (Segev & Shapiro 1982; Weide *et al.* 1989) still await experimental confirmation.

The use of photofragment mapping to probe the intramolecular dynamics of polyatomic molecular dissociation processes came of age with the advent of tunable, narrow line, polarized laser pump-probe techniques, which reveal the intramolecular stereo-dynamics in unprecedented detail (Houston 1987; Simons 1987; Faraday Symposium 1989), usually following direct excitation into the electronically excited continuum. The parallel development of femtosecond pump-probe techniques (Roster *et al.* 1988; Zewail 1989) is providing unique insight into the time-resolved dynamics of the dissociating molecule. Full state-to-state resolution of the dissociation process can be achieved if the continuum is accessed via predissociation from a rotationally structured excited electronic state, e.g. $H_2O(\tilde{C}^1B_1)$ (Docker *et al.* 1987), $H_2CO(S_1)$ (Butenhoff *et al.* 1989), or by adopting a double resonance strategy involving prior infrared excitation into specific rovibrational levels in the ground state, e.g. $H_2O(\tilde{X}^1A_1, (0,0,1))$ (Häusler *et al.* 1987). Of course, the prior excitation need not be restricted to fundamental transitions lying in the infra red, but can be extended to higher overtones; in particular, when the overtones are associated with local mode, X–H vibrations, the molecule can be prepared in very highly excited rovibrational levels (Ticich *et al.* 1987). Their subsequent dissociation, promoted by absorption of a second photon (usually but not necessarily of the same colour) has been termed vibrationally mediated photodissociation (Ticich *et al.* 1987) or VIMP.

Phil. Trans. R. Soc. Lond. A (1990) **332**, 245–258 *Printed in Great Britain*

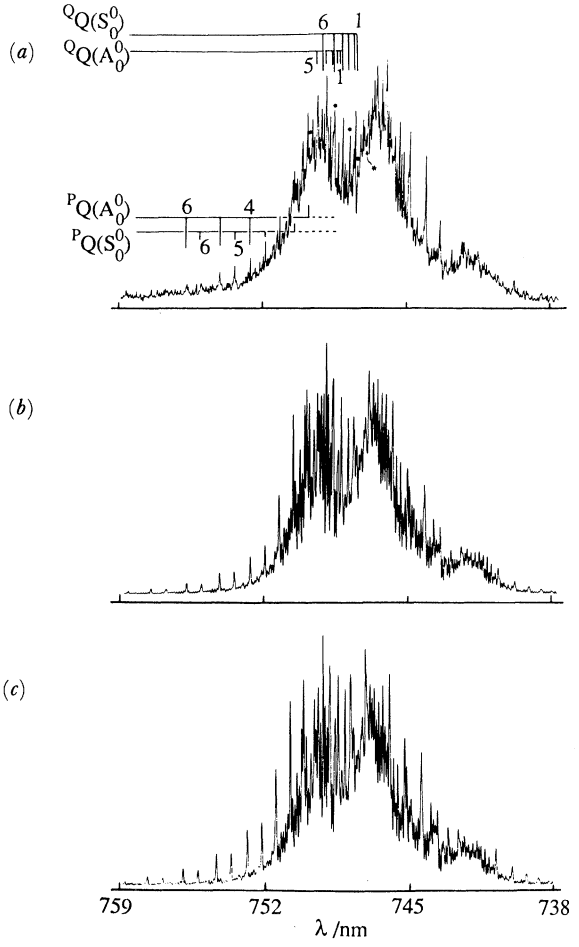

Figure 1. Rotational contours of the absorption bands in HOOH at 298 K associated with excitation into the third O–H overtone level at wavelengths *ca.* 748 nm. (*a*) Experimental VIMP photofragment yield spectrum recorded at a laser-line width of 0.15 cm^{-1}, via the LIF intensity of the $Q_1(6)$ feature in the OH(A–X) band. (*b*) Simulated absorption spectrum assuming an isotropic distribution over the population of vibrationally excited molecules. (*c*) As (*b*), but assuming the retention of the alignment initially conferred on the excited molecular populations. The filled circles and the asterisk indicate the selected band-heads listed in table 1, with the asterisk corresponding to excitation at 748.01 nm.

The efficiency of VIMP is amplified by the greatly enhanced cross-section for secondary photon absorption at long wavelengths. This can occur because the local X–H vibrational mode runs parallel to the reaction–dissociation coordinate, e.g.

$$H_2O|4O\rangle^- + h\nu \rightarrow H + OH \qquad (1.1)$$

(vander Wal & Crim 1989) or because the local mode is contaminated by contributions from other vibrational motions that have components along the reaction coordinate, e.g.

$$H_2O_2|4O\rangle^- + h\nu \rightarrow OH + OH \qquad (1.2)$$

(Ticich *et al.* 1987; Likar *et al.* 1988; Brouard *et al.* 1989, 1990*a*). (The label $|4O\rangle^-$

denotes the antisymmetric local mode state, associated with four quanta of O–H stretching.) In either case, if the second photon is of low energy, Franck–Condon constraints ensure preparation of the dissociating, electronically excited molecule at bond extensions well on the way to the dissociation limit (Likar *et al.* 1988; Brouard *et al.* 1989) where the slope of the interfragment potential and its angular anistropy are greatly reduced. Under these conditions, the final quantum state distributions, and linear and angular momentum disposals in the separated fragments largely reflect the character and intramolecular motions in the intermediate, vibrationally excited state of the parent molecule. Vibrationally mediated photodissociation provides a means of 'interrogating' highly excited overtone states via 'photofragment mapping' (Brouard *et al.* 1990*a*).

This strategy has been adopted in studying the intramolecular behaviour of selected groups of rovibrational states in HOOH and HOOD, populated by absorption of tunable, pulsed laser radiation at wavelengths *ca.* 750 nm. The 'interrogated' molecules, excited via the $4\nu_{\mathrm{O-H}}$ 'local mode' transition have been probed through measurements of photofragment quantum state distributions and vector correlations; of their scalar vibrational (v_1, v_2) and rotational $(N_1, \langle N_2 \rangle)$ pair correlations; and of their dependence (or otherwise) on the initial sets of $|J, K_a\rangle$ rotational states populated in the overtone level. Amongst the central questions addressed are: (i) the rovibrational character of the 'interrogated' molecules; (ii) the importance of rotation–vibration coupling in the intermediate state; and, (iii) the role of the dissociative continuum in the 'interrogation' process.

2. Experimental

The experimental techniques used in the polarized, Doppler-resolved probing of single colour vibrationally mediated photodissociation have been fully described (Brouard *et al.* 1989). The $4\nu_{\mathrm{O-H}}$ stretching overtones ($|4\mathrm{O}\rangle^-$ in the local mode description) in HOOH and HOOD were prepared and interrogated through the sequential absorption of polarized photons, from a tunable pulsed laser at wavelengths *ca.* 750 nm. The average interval between absorption of the 'preparation' and 'interrogation' photons, which depends on the photon flux and the secondary photon absorption cross-sections, is estimated to lie in the range 100–500 ps. The population distributions, velocities and angular vector correlations in the recoiling OH(OD) fragments were probed via sub-Doppler, laser induced fluorescence (LIF) spectroscopy of the (0, 0) and (1, 1) bands of the OH(OD) $A^2\Sigma^+ - X^2\Pi$ system. Analysis of the Doppler profiles of selected rotational features in the LIF spectra followed the procedures discussed earlier (Dixon 1986; Brouard *et al.* 1990*a*).

3. Preparation and characterization of the intermediate overtone state

The overtone transition in HOOH, centred at wavelengths around 750 nm displays a rich rotational structure which includes both type a and type b components. These give rise to clearly resolved progressions of ${}^{\mathrm{Q}}\mathrm{Q}(K)$ ($\Delta K = 0$, $\Delta J = 0(K)$) and ${}^{\mathrm{P,R}}\mathrm{Q}(K)$ sub-band branch-head progressions respectively, see figure 1. The type a component contributes 80% of the intensity (Douketis & Reilly 1989). The level splitting introduced by the torsional barrier, introduces further complexity into the spectrum which includes contributions from two principal vibrational transitions, designated S_0^0 and A_0^0 (Dübal & Crim 1985); weaker,

torsionally excited sequence bands comprising the S_1^1 and A_1^1 transitions contribute additional intensity on the high frequency side. The transition dipole has a high degree of local mode, H–O stretching character (Douketis & Reilly 1989).

The rotational structure shown in figure 1 has been assigned on the basis of asymmetric top band contour calculations; these incorporate the rotational constants and centrifugal distortion parameters for the S_0^0 component (Douketis & Reilly 1989) and similar sets of parameters for the A_0^0 and sequence bands. Although the selective excitation of single rovibrational features was precluded at the bandwidth of the laser used (*ca.* 0.15 cm^{-1}), the resolution was sufficient to allow a very high degree of K_a selectivity. The spectral simulations were used to identify the dominant transitions contributing to each selected band-head, and these together with the average values for J, are listed in table 1. The majority of experiments were conducted at 748 nm. The other wavelengths were selected to probe any sensitivity of the VIMP dynamics to the prior choice of K_a.

The initial degree of alignment conferred upon the vibrationally excited molecular population, depends on the choice of band-head, e.g. ^{Q}Q or $^{P,R}Q$, and the initial $|J, K_a\rangle$ selection. If this alignment were still wholly, or partly retained at the instant of secondary photon absorption (interrogation) the intensity distribution in the photofragment yield spectrum would differ from that calculated assuming an isotropic population. Parent molecular alignment in the intermediate state would also affect the shapes of the Doppler profiles in LIF spectra of the recoiling photofragments. Although the intensity distributions in the calculated yield spectra are similar to those in the published (non-aligned) absorption spectra (Douketis *et al.* 1989), the spectral simulations are not yet sufficiently refined to allow a clearly unambiguous distinction between the spectra predicted for aligned against isotropic populations in the intermediate rovibrational states. However, the translational anisotropy of the recoiling fragments, calculated via Doppler analysis of the $R_2(1)$ features, was found to be independent of the choice of parallel against orthogonal excitation-detection geometries (Brouard *et al.* 1990*a*) or of the prior selection of $^{P,R}Q$ against ^{Q}Q features in the overtone transition, which suggests that the initial molecular alignment in the LAB frame is fully destroyed before interrogation, presumably through vibrational–rotation coupling. This view is greatly reinforced by a parallel insensitivity of the photofragment vector correlations (determined from analysis of the Doppler profiles) and the scalar (v_1, v_2), $(N_1 \langle N_2 \rangle)$ pair correlations to the initial state selection, see the discussion in §4(*b*).

4. Photofragment mapping of intramolecular dynamics

(*a*) *Characterizing the continuum*

In the VIMP experiment, the interrogating photon projects the intermediate overtone state onto an upper electronic continuum (or continua) subject to the constraints of the Franck–Condon Principle. In this sense the upper continuum state acts as a kind of lens through which the character of the intermediate overtone state is viewed and the nature of the image it projects depends on the wavelength of the interrogating photon. The motion of the separating fragments also includes a contribution from the dynamics on the repulsive potential energy surface, which may blur the projected image of the intramolecular dynamics operating in the interrogated population of vibrationally excited molecules. It is essential, therefore, to characterize the shape of the 'projecting lens', through single photon direct

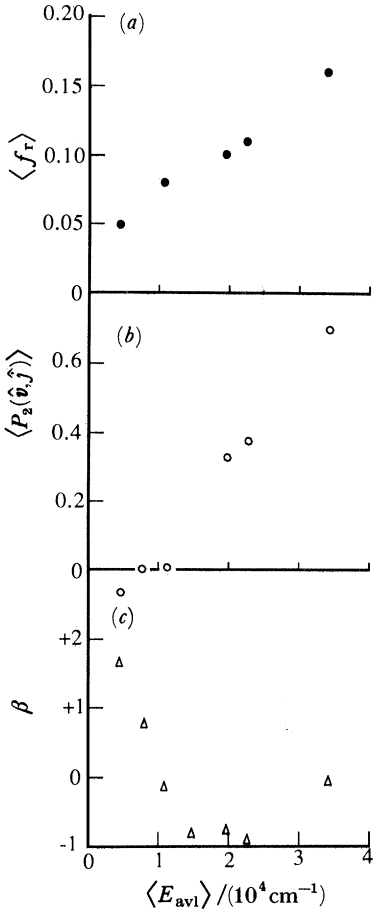

Figure 2. Wavelength/photon energy dependence of (*a*) the average fraction of energy released into fragment rotation, $\langle f_r \rangle$, (*b*) the photofragment vector correlation, $\langle P_2(\hat{v}_{OH}, \hat{j}_{OH}) \rangle$, and (*c*) the translational anisotropy, β, in the direct single photon dissociation of HOOH. $\langle E_{avl} \rangle$ represents the maximum energy available for disposal among the recoiling OH fragments.

Table 1. *Rotational assignment of selected band heads in the third* O–H *stretching overtone transitions of* HOOH

λ/nm	principal transitions, $^{\Delta K_a}\Delta J(K_a)$	$\langle J \rangle$
748.01	^{Q}R(4) (S_0^0), 70%; ^{Q}R(5) (A_0^0), 30%	12
748.20	^{Q}Q(1) (S_0^0), 40%; ^{Q}R(5) (S_0^0), 43%; ^{Q}R(4) (A_0^0), 17%	7
748.55	^{Q}Q(3) (S_0^0)	7
749.24	^{Q}Q(5) (S_0^0), 70%; ^{Q}P(1) (S_0^0), 30%	9
750.24	^{Q}P(1) (S_0^0), 60%; ^{Q}P(2) (A_0^0), 40%	11

photodissociation studies, before applying the strategy of photofragment mapping to the VIMP experiment (Crim 1988; Simons 1988). Similar considerations apply in the time resolved probing of direct photodissociation dynamics, via femtosecond kinetic spectroscopy (Zewail 1989; Bernstein & Zewail 1989).

Figure 2 summarizes the results of a series of single-photon experiments, conducted at wavelengths extending further and further into the long wavelength edge of the

Table 2. *Average energy disposals in the vibrationally mediated photodissociation of* HOOH(D) *at 748* nm (*energies in* cm^{-1})

channel		branching function	$\langle E_r \rangle$	$\langle E_v \rangle$	$\langle E_t \rangle$
HOOH	$OH(v=0)+OH(v=0)$	0.78	1700	0	8620
	$OH(v=0)+OH(v=1)$	0.22	1080	3570	6210
	average		1560	790	8090
HOOD	$OH(v=0)+OD(v=0)$	0.76	1410 (OH)	O (OH)	7700
			1030 (OD)	O (OD)	
	$OH(v=1)+OD(v=0)$	0.12	520 (OH)	3570 (OH)	—
			360 (OD)	0 (OD)	
	$OH(v=0)+OD(v=1)$	0.12	700 (OH)	0 (OH)	—
			490 (OD)	2630 (OD)	
	average		1250 (OH)	428 (OH)	—
			890 (OD)	316 (OD)	

electronic absorption continuum of HOOH (Brouard *et al.* 1990*b*). At short wavelengths where the anisotropy in the excited interfragment potential is strong (Schinke & Staemmler 1988) the fraction of energy released into rotation, $\langle f_r \rangle$, is relatively high. The positive value of the vector correlation $\langle P_2(\hat{\boldsymbol{v}}_{OH}, \hat{\boldsymbol{j}}_{OH}) \rangle$ betrays the important role of torsion about the HO–OH bond ($\hat{\boldsymbol{v}}_{OH}$ and $\hat{\boldsymbol{j}}_{OH}$ are the unit velocity and rotational angular momentum vectors of the separated OH fragments respectively). No energy is released into vibration. As the photon energy is reduced, however, and the fragment separation is initiated at HO–OH distances closer and closer to the dissociation limit, $\langle f_r \rangle$ steadily falls and the vector correlation ($\hat{\boldsymbol{v}}_{OH}, \hat{\boldsymbol{j}}_{OH}$) disappears. The molecule behaves increasingly as if it were diatomic.

The changes in the translational anisotropy β, reveal an unexpected subtlety; the variations in its magnitude and sign reflect varying contributions from two distinct continuum states, one accessed by transitions polarized perpendicular to the dissociating bond, the other near parallel to it, and assigned to the $\tilde{A}^1A$ (*trans*) and $\tilde{B}^1B$ (*cis*) states respectively (Chevaldonnet *et al.* 1986; Schinke & Staemmler 1988). In the single photon experiment the spread of values for β spans nearly all the permissible range, $+1.7 \geqslant \beta \geqslant -1$; in the VIMP experiment, the intermediate value of $\beta \approx -(0.3\text{–}0.5)$ again reflects contributions from two continuum states though their relative contributions are not identical to those predicted for single photon excitation at the same equivalent energy.

When the upper state continuum is accessed via the intermediate overtone state, $4\nu_{O-H}$ in a VIMP experiment at *ca.* 748 nm, the rotational energy disposal rises dramatically, the ($\hat{\boldsymbol{v}}_{OH}, \hat{\boldsymbol{j}}_{OH}$) correlation returns, and 11 % of the OH fragments carry one quantum of vibration (Likar *et al.* 1988; Brouard *et al.* 1989, 1990*a*). The change is even more dramatic for HOOD, where the fraction of energy in rotation, $\langle f_R \rangle = 0.22$ and 12 % of the fragments carry vibrational excitation, see table 2; note the near equally probable vibrational excitation of both OH and OD.

Since the residual anisotropy in the electronically excited continuum at large O–O extensions can only provide very minor additional torques to the separating fragments, the observed rotational distributions and directional correlations must reflect very largely, the angular motions in the intermediate vibrational overtone state. These could include symmetric and antisymmetric HOO(DOO) bending vibrations, and torsion together with parent molecular rotations, J_a, about the O–O axis: (rotation about the orthogonal b and c inertial axes will be converted

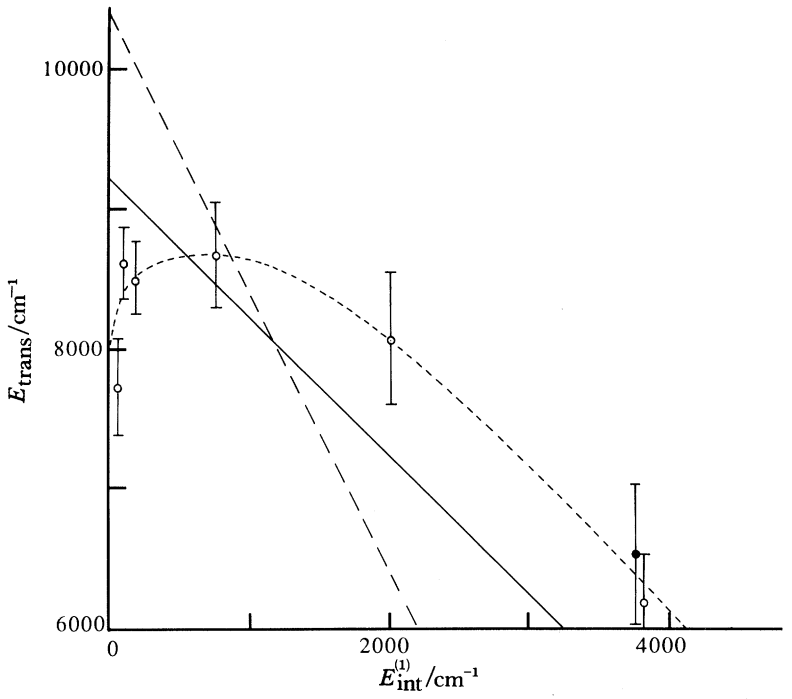

Figure 3. Vibrationally mediated photodissociation of HOOH at 748 nm; quantum state dependence of the mean energy released into translation, $\langle E_{\mathrm{t}}\rangle$, in $\mathrm{OH}(N_1)_{v=0}$. ——, dependence assuming $E_{\mathrm{int}}(2) = \langle E_{\mathrm{int}}(1)\rangle$; – – –, dependence assuming $E_{\mathrm{int}}(2) = E_{\mathrm{int}}(1)$; ○, OH ($v = 0$); ●, OH($v = 1$).

Table 3. *Average rotational energies associated with* OH(D) $v = 0$ *fragments, aligned with* $\boldsymbol{j}\|\boldsymbol{v}(\langle E_{\mathrm{r}}\rangle^{\|})$ *and* $\boldsymbol{j} \perp \boldsymbol{v}(\langle E_{\mathrm{r}}\rangle^{\perp})$, *generated through overtone mediated photodissociation at 748* nm (*energies in* cm^{-1})

	fragment	$\langle E_{\mathrm{R}}^{\|}\rangle$	$\langle E_{\mathrm{R}}^{\perp}\rangle$
HOOH	OH	425 ± 50	425 ± 50
HOOD	OH	700 ± 120	700 ± 120
	OD	405 ± 110	625 ± 110

principally into orbital angular momentum). The balance between their relative contributions dictates, to a good approximation, the components of rotational angular momentum, $\langle j^2\rangle^{\|}$ and $\langle j^2\rangle^{\perp}$, directed parallel and perpendicular to the recoil velocity vector **v** and hence the sign and magnitude of the $(\hat{\boldsymbol{v}}, \hat{\boldsymbol{j}})$ correlation. The relative values of the corresponding energies calculated in the classical high j limit and averaged over the final product rotational state distributions (Brouard *et al.* 1990*a*) are listed in table 3. Strikingly, in HOOD, $\langle E_{\mathrm{OH}}^{\perp}\rangle > \langle E_{\mathrm{OD}}^{\perp}\rangle$; if the perpendicular component had been generated by an impulsive torque in the final continuum (cf. the behaviour found is the direct single photon dissociation of DOOD at 266 nm (Gericke *et al.* 1988)) rather than by the transformation of angle bending vibrational kinetic energy in the intermediate state, the opposite behaviour would have resulted. In the following analysis the photofragment mapping of intramolecular motions is taken to reflect exclusively the character of the intermediate overtone state at the wavelength selected for its interrogation.

(*b*) *Resolving the motions in the intermediate overtone state*

Particularly detailed insight into the origin of fragment rotation can be gained through determination of the scalar rotational fragment pair correlations, (N_1, $\langle N_2 \rangle$), since they are controlled by the balance between a-axis rotation and torsional motion, and between the symmetric and antisymmetric bending vibrations in the intermediate state. The scalar pair correlations have been determined in the HOOH system initially excited into the ^{Q}R branches ($K_a = 4, 5$) through analysis of the Doppler-resolved profiles of selected rotational features in the LIF spectrum of the separated OH fragments. Figure 3 displays the variations in their average translational energies $\langle E_t \rangle$ (determined on the assumption of a single recoil velocity), with the internal energy, $E_{int}(1)$, of the probed OH fragment, hereby designated as fragment 1. Also shown are the expected trends in the translational energy $\langle E_t \rangle$, if the mean internal energy in the 'unobserved' sister fragment, $\langle E_{int}(2) \rangle$, were either equal to that of the selected fragment, $E_{int}(1)$ or remained constant, independent of the level probed in fragment 1. The experimental variation of $\langle E_t \rangle$ obviously does not conform to either model, but instead displays an anti-correlation between the internal energies in the 'observed' OH(1), and 'unobserved' OH(2) fragments: low internal excitation in OH(1, 2) correlates with high excitation in OH(2, 1).

A more detailed analysis, which explores the consequences of various model distributions, $W(i)$ among the vibrational and rotational quantum states i of the unobserved sister fragments OH(2), provides a quantitative insight into the nature and origin of the observed anti-correlation (Brouard *et al.* 1990*c*). The distributions of recoil velocities $W(v_i)$, associated with alternative model distributions of the internal energy $E_{int}(2)$ in OH(2), were calculated via the equation:

$$v_i = \{2[E_{avl} - E_{int}(1) - E_{int}(2)]/m_{OH}\}^{\frac{1}{2}}, \tag{4.1}$$

E_{avl} represents the total available energy at the wavelength of the absorbed photons and m_{OH} is the mass of the fragment; $E_{avl} - E_{int}(1)$ thus represents the maximum energy available for release into translation. In the Doppler profile fitting procedure (for a given model distribution $W(i)$), the optimized parameters E_{avl} and β_{eff} (the effective translational anisotropy associated with that profile) were those that gave the best fit for the set of velocities $\{v_i\}$. The returned estimate of E_{avl} necessarily depends on the trial distribution $W(i)$, but an acceptable trial distribution is subject to strong constraints. E_{avl} has to be independent of the state selected in the probed fragment OH(1), and to lie close to the range of values estimated on the basis of thermochemical data. In addition the energy averaged over the model distribution in OH(2) has to equal that in OH(1), while the overall internal state distribution must agree with that observed experimentally at Wisconsin (Likar *et al.* 1988) or Nottingham. The imposition of these constraints led to the following conclusions.

1. OH ($v = 1$) fragments have partners born exclusively in low rotational states of OH ($v = 0$).

2. The two product vibrational channels, OH ($v = 0$) + OH ($v = 0$) and OH ($v = 1$) + OH ($v = 0$) have different rotational distributions, with maximum populations in levels $N = 6$ and $N < 3$ respectively.

3. The internal energy correlation observed in the OH ($v = 0$) fragments is due predominantly to a rotational state anti-correlation in the OH ($v = 0$) + OH ($v + 0$) channel, see table 4.

PHILOSOPHICAL TRANSACTIONS OF THE ROYAL SOCIETY A MATHEMATICAL, PHYSICAL & ENGINEERING SCIENCES

Table 4. *Rotational fragment pair correlations* $(N_1, \langle N_2 \rangle)$ *for* OH *fragments generated in the vibrationally mediated photodissociation of* HOOH *at 748* nm

		$\langle N_2 \rangle$	
N_1		$K_a \approx 4$	$K_a \approx 1$
$V=0$	1	9 ± 1	—
	2	11 ± 1	—
	3	8 ± 1	8 ± 1
	6	3 ± 2	8^{+1}_{-2}
	10	5^{+1}_{-3}	1^{+2}_{-1}
	12	—	3^{+1}_{-3}
	14	4^{+1}_{-3}	—
$V=1$	$N=3$	3 ± 2	—

Experiments were also conducted with alternative initial selections of K_a in the overtone state with values of $K_a = 1 \rightarrow 4, 5$, selected by tuning the laser frequency to different sub-band heads, see table 1. Neither the fragment pair correlations $(N_1, \langle N_2 \rangle)$, nor the effective translational anisotropies β_{eff} (and hence the $(\hat{\boldsymbol{v}}, \hat{\boldsymbol{j}})$ correlations) were significantly changed by variations in the initial choice of K_a, see table 4. Such behaviour would not have been followed, had the intramolecular motion in HOOH approximated that of a rigid, uncoupled near prolate symmetric rotor. In order to understand both the origin of the $(N_1, \langle N_2 \rangle)$ correlations and their insensitivity to the initial K_a selection, it is helpful to review first the $(N_1, \langle N_2 \rangle)$ correlations found in the direct, single photon dissociation of H_2O_2 at 193 nm (Gericke 1988), and their modelling via classical trajectory calculations (Schinke 1988; Schinke & Staemmler 1988).

When H_2O_2 is jet cooled, so that only low K_a levels are populated, the generation of fragment rotation is largely determined by torsional motion in the electronically excited continuum state: angular momentum conservation ensures $N_1 = \langle N_2 \rangle$. At 300 K, where the population spreads to higher levels of K_a, the additional angular momentum reinforces the rotation of one fragment but opposes that of the other and in consequence, the direct correlation is destroyed and the overall rotational population distribution is broadened. Further increase of temperature, raising $\langle K_a \rangle$ still further, should eventually promote an anti-correlation, as found in the present two photon, vibrationally mediated experiments. The $(N_1, \langle N_2 \rangle)$ correlation provides a thermometer for the measurement of the a-axis rotational temperature in the interrogated parent molecule. Under VIMP conditions, where the magnitude of the positive $(\hat{\boldsymbol{v}}, \hat{\boldsymbol{j}})$ correlation in the rotationally excited fragments reflects a much stronger contribution from symmetric and antisymmetric bending, similar arguments still apply.

The observed distributions and correlations can be simulated by adopting a classical mechanical model, similar to that used by Vasudev *et al.* (1984) (Brouard *et al.* 1990*c*). Angular vibrational motions in the interrogated molecule (or its electronic continuum, in the direct single photon dissociation experiments) are assumed to generate separate gaussian distributions over angular momentum in the photofragments; a axis rotation (which maps into fragment rotation with unit efficiency) is described either by a Boltzmann distribution over K_a states (direct dissociation) or by a single, average value of K_a (vibrationally mediated dissociation). Vector addition of the a axis and torsional contributions to the product angular

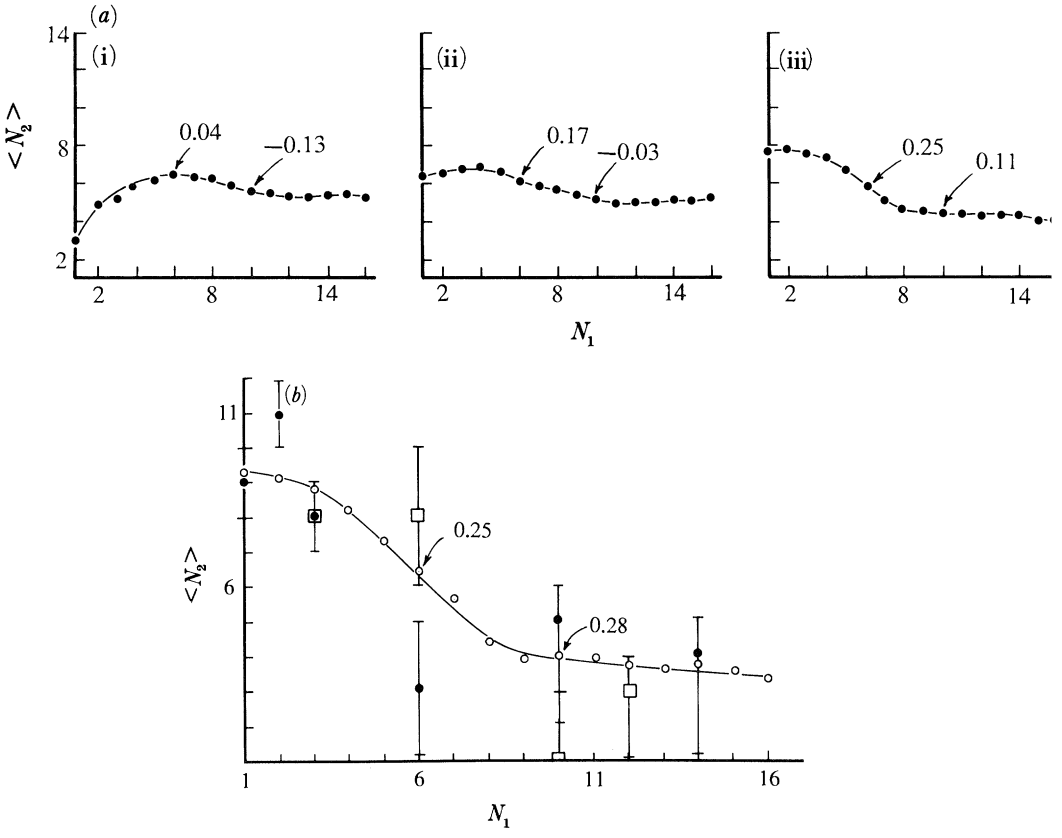

Figure 4. Simulated rotational fragment pair correlations (N_1, $\langle N_2 \rangle$) for the vibrationally mediated dissociation of HOOH (*a*) when $\langle K_a \rangle = 1$ (i), 3 (ii) or 5 (iii), and (*b*) $\langle K_a \rangle = 7$. The arrowed numbers are calculated values for the $(\hat{\boldsymbol{v}}, \hat{\boldsymbol{j}})$ correlation (the experimental value for OH($N = 10$) is $+0.23$). The filled circles and squares indicate the experimental data obtained at 748.01 nm, for which the initial value of $\langle K_a \rangle \approx 4$, 5, and at 750.24 nm, where the initial value of $\langle K_a \rangle \approx 1$.

momentum, and where appropriate, of the symmetric and antisymmetric bending contributions, allows determination of the final (N_1, $\langle N_2 \rangle$) correlations. The model was initially tested by simulating the direct, single-photon dynamics reported by Grunewald *et al.* (1987) and Gericke (1988). The widths and means of the gaussian angular momentum components were first optimized to reproduce the experimental $(\hat{\boldsymbol{v}}, \hat{\boldsymbol{j}})$ correlations, overall rotational distributions and (N_1, $\langle N_2 \rangle$) correlations measured under jet-cooled conditions, where $K_a \approx 0$. The simulations were then repeated for the dissociation at 298 K, but this time only the distribution over K_a states was changed. The resulting overall rotational distributions, as well as the scalar and vector correlations accurately reproduced those determined experimentally (Grunewald *et al.* 1987; Gericke 1988), or predicted via classical trajectory calculations (Schinke 1988; Schinke & Staemmler 1988).

Satisfactory simulations of the corresponding sets of data obtained in the two photon, vibrationally mediated experiments was obtained, provided each of the four possible types of parent angular motion were allowed to contribute equally to the generation of fragment rotation, with $\langle K_a \rangle \approx 7$, see figure 4. Reduction of the *a* axis angular momentum to $\langle K_a \rangle = 1$ (keeping the other contributions constant)

Table 5. *Average energy distributions in* HOOH, HOOD ($4\nu_{O-H}$) *interrogated by photodissociation at* 748 nm (*energies in* cm^{-1})

mode	dissociation channel		
HOOH	OH($v=0$)+OH($v=0$)	OH($v=1$)+OH($v=0$)	
O–H stretch	0	3570	
O–O stretch	10300	7600	
HOO bend	1780	1100	
torsion	900	1100	
a axis rotation	400		
HOOD	OH($v=0$)+OD($v=0$)	OH($v=1$)+OD($v=0$)	OH($v=0$)+OD($v=1$)
O–H stretch	0	3570	0
O–D stretch	0	0	2630
O–O stretch	8400	7940	8260
OOH bend	1470	610	740
OOD bend	1380	530	670
torsion	2050	700	1070
a axis rotation	(150±150)	—	—

dramatically altered both the $(\hat{\boldsymbol{v}}, \hat{\boldsymbol{j}})$ and $(N_1, \langle N_2 \rangle)$ correlations, in striking contrast to the insensitivity observed experimentally, see table 4. The discrepancy arises because the model neglects the contribution from rotational–vibrational coupling in the vibrationally excited H_2O_2.

The resolution of the components of intramolecular motion that are converted into fragment rotation enables their average energies to be determined (Vasudev *et al.* 1984; Brouard *et al.* 1990*a*). These are listed in table 5. The remaining entries have been estimated by treating the H–O stretch as adiabatic, so that generation of OH(v) implies the excitation of v quanta of H–O stretch in the interrogated parent molecule. The energy assigned to O–O stretching is that required for total energy conservation. Similar results, obtained for HOOD (Brouard *et al.* 1990*a*) are also shown, for completeness.

(*c*) *Discussion*

Under the conditions of the present experiments, which use nano-second laser pulses, the vibrational excitation in the interrogated overtone state will be delocalized, (Stewart & McDonald 1981, 1983; Leone & Nesbitt 1982) despite the localization of the transition associated with the photon absorption (Holme & Hutchinson 1986; Hutchinson & Marshall 1986, 1988). The average interval between absorption of the 'preparation' and 'interrogation' photons, estimated to lie in the range *ca.* (100–500) ps, should be longer than the characteristic time for IVR (though possibly not a great deal longer in the light of recent estimates based on quasiclassical trajectory calculations (Getino *et al.* 1989)) and the insensitivity of the quantum state distributions and correlations in the photofragments to changes is the 'preparation–interrogation' photon flux at 748 nm, reinforce this view. At this long wavelength, where the total absorbed energy is not too far above the dissociation threshold the Franck–Condon principle ensures that the image of the intermediate state character favours vibrational components that were 'unseen' in the preparation stage. Different wavelengths, necessarily, will project different images: witness the enhanced proportion of vibrationally excited OH fragments, generated by interrogation at 532 nm rather than 748 nm (Likar *et al.* 1988). At shorter wavelengths

still, the Franck–Condon factors associated with H–O stretching vibrations should assume still greater importance, perhaps introducing competition between the alternative channels

$$\mathrm{HOOH} \longrightarrow \begin{cases} \rightarrow \mathrm{OH} + \mathrm{OH} & (4.2) \\ \rightarrow \mathrm{HO_2} + \mathrm{H} & (4.3) \end{cases}$$

and the involvement of more highly excited continua.

Several theoretical papers have emphasized the anticipated importance of rotational–vibrational coupling in promoting IVR in HOOH and related molecules such as HONO (Sumpter & Thomson 1988; Sumpter *et al.* 1988; Guan & Thompson 1989). In particular, the coupling of torsional motion with a axis rotation has been highlighted (Sumpter *et al.* 1988), together with the breakdown of K as a good quantum number (Parmenter 1983; Salhn & Uzer 1989). Many of the experimental results obtained in the present work support these predictions. These include the following:

1. The loss of the rotational alignment initially conferred upon the vibrationally excited molecular population, during the interval between preparation and interrogation. This recalls the depolarization of rotationally aligned fluorescent polyatomic molecules, associated with intramolecular vibrational–rotational energy redistribution during the fluorescent lifetime (IVRET) (Nathanson & McClelland 1984).

2. The contribution of a axis rotational angular momentum to the rotational excitation of the OH(D) fragments. The rotational pair (anti) correlation data for HOOH molecules, initially excited into levels with $\langle J \rangle \approx 12$ and $\langle K_a \rangle \approx 4, 5$, can be modelled if the interrogated molecules have $\langle K_a \rangle \approx 7 \pm 1$. An isotropic distribution of HOOH molecules at 300 K, would have $\langle J \rangle \approx 12$ and $\langle K_a \rangle \approx 7$.

3. The insensitivity of the observed dynamical behaviour to the selection of alternative initial levels with values of K_a ranging from $K_a = 1 \rightarrow 5$. Clearly K is not a good quantum number, although it appears to be in the modelling of the K sub-band structure associated with the S_0^0 band. Appearances may be deceptive, however: it has not been possible to analyse the rotational structure of the A_0^0 band, recorded at high resolution, on a similar basis, (Douketis & Reilly 1989) presumably because of the enhanced perturbations introduced by rotational–vibration coupling.

Experiments conducted on shorter timescales may allow sampling of the intermediate state character while it is still evolving. The density of states in HOOH and HOOD excited into the third overtone, $4\nu_{\mathrm{O-H}}$, remains relatively small (a few states per cm^{-1}) and the projected IVR times are relatively long (Getino *et al.* 1989); thus single colour experiments using high intensity picosecond pulses to provide average preparation–interrogation times in the sub-picosecond range should be fast enough to reveal intensity- and time-dependent variations in the interrogated molecular alignments and photofragment dynamics. Alternatively two colour experiments, utilizing tunable radiation at *ca.* 750 nm and a variably delayed interrogation pulse at 532 nm, will allow measurements to be made in the range 10–1000 ps.

We are most grateful to Coherent (U.K.) Ltd for the generous loan of a dye laser and to SERC for a research grant. We have also learnt much through helpful discussions with Professor R. N. Dixon and especially through correspondence and discussion with Professor F. F. Crim.

References

Bernstein, R. B. & Zewail, A. H. 1989 *J. chem. Phys.* **90**, 829–842.

Brouard, M. 1989 *J. chem. Soc. Faraday Trans.* II **85**, 1295–1297.

Brouard, M., Martinez, M. T., O'Mahony, J. & Simons, J. P. 1989 *J. chem. Soc. Faraday Trans.* II **85**, 1207–1220.

Brouard, M., Martinez, M. T., O'Mahony, J. & Simons, J. P. 1990*a* *Molec. Phys.* (In the press.)

Brouard, M., Martinez, M. T., Milne, C. J., Simons, J. P. & Wang, J. X. 1990*b* *Chem. Phys. Lett.* (In the press.)

Brouard, M., Martinez, M. T. & O'Mahony, J. 1990*c* *Molec. Phys.* (Submitted.)

Butenhoff, T. J., Carleton, K. L., Chuang, M. C. & Moore, C. B. 1989 *J. chem. Soc. Faraday Trans.* II **85**, 1155–1168.

Carrington, T. 1964 *J. chem. Soc. Faraday Trans.* II **84**, 1627–1628.

Chevaldonnet, C., Cardy, H. & Dargelos, A. 1986 *Chem. Phys.* **102**, 55–61.

Crim, F. F. 1988 *J. chem. Soc. Faraday Trans. II* **84**, 1627–1628.

Dixon, R. N. 1986 *J. chem. Phys.* **85**, 1866–1879.

Docker, M. P., Hodgson, A. & Simons, J. P. 1987 High resolution photochemistry: In *Molecular photodissociation dynamics, advances in gas phase photochemistry and kinetics* (ed. M. N. R. Ashfold & J. E. Baggott), pp. 115–137. Royal Society of Chemistry.

Douketis, C. & Reilly, J. P. 1989 *J. chem. Phys.* **91**, 5239–5250.

Dübal, H.-R. & Crim, F. F. 1985 *J. chem. Phys.* **82**, 3863–3872.

Faraday Symposium 1989 Orientation and polarisation effects in reactive collisions. *J. chem. Soc. Faraday Trans.* II **85**, 925–1376.

Gericke, K. H. 1988 *Phys. Rev. Letts.* **60**, 561–564.

Gericke, K. H., Golzenleuchter, H. & Comes, F. J. 1988 *Chem. Phys.* **127**, 399–409.

Getino, C., Sumpter, B. G., Santamaria, J. & Ezra, G. S. 1989 *J. phys. Chem.* **93**, 3877–3880.

Grunewald, A. H., Gericke K.-H. & Comes, F. J. 1987 *J. chem. Phys.* **87**, 5709–5721.

Guan, Y. & Thompson, D. L. 1989 *Chem. Phys.* **139**, 147–161.

Häusler, D., Andresen, P. & Schinke, R. 1987 *J. chem. Phys.* **87**, 3949–3965.

Holme, T. A. & Hutchinson, J. S. 1986 *J. chem. Phys.* **84**, 5455–5462.

Houston, P. L. 1977 *J. phys. Chem.* **91**, 5388–5397.

Hutchinson, J. S. & Marshall, K. T. 1988 *J. chem. Soc. Faraday Trans.* II **84**, 1535–1554.

Leone, S. R. & Nesbitt, D. J. 1982 *Chem. Phys. Lett.* **87**, 123–127.

Likar, M. D., Baggott, J. E., Sinha, A., Ticich, T. M., vander Wal, R. L. & Crim, F. F. 1988 *J. chem. Soc. Faraday Trans.* II **84**, 1483–1497.

Nathanson, G. M. & McClelland, G. M. 1984 *J. chem. Phys.* **81**, 629–642.

Neujmin, H. & Terenin, A. 1934 *Nature, Lond.* **134**, 255.

Parmenter, C. S. 1983 *Faraday Discuss. chem. Soc.* **75**, 7–32.

Roster, M. J., Dantus, M. & Zewail, A. H. 1988 *J. chem. Phys.* **89**, 6113–6140.

Sahm, D. K. & Uzer, T. 1989 *Chem. Phys. Lett.* **163**, 5–10.

Schinke, R. 1988 *J. phys. Chem.* **92**, 4015–4019.

Schinke, R. & Staemmler, V. 1988 *Chem. Phys. Lett.* **145**, 486–492.

Segev, E. & Shapiro, M. 1982 *J. chem. Phys.* **77**, 5604–5623.

Simons, J. P. 1987 *J. phys. Chem.* **91**, 5378–5387.

Simons, J. P. 1988 *J. chem. Soc. Faraday Trans.* II **84**, 1624–1626.

Simons, J. P., Brouard, M., Martinez, M. T., O'Mahony, J. & Wang, J. X. 1989 *J. chem. Soc. Faraday Trans.* II **85**, 1315–1318.

Stewart, G. N. & McDonald, D. J. 1981 *J. chem. Phys.* **75**, 5949–5950.

Stewart, G. N. & McDonald, D. J. 1983 *J. chem. Phys.* **78**, 3907–3915.

Sumpter, B. G. & Thompson, D. L. 1988 *Chem. Phys. Lett.* **153**, 243–252.

Sumpter, B. G., Martens, C. C. & Ezra, G. S. 1988 *J. phys. Chem.* **92**, 7193–7204.

PHILOSOPHICAL TRANSACTIONS OF THE ROYAL SOCIETY A MATHEMATICAL, PHYSICAL & ENGINEERING SCIENCES

Ticich, T. M., Likar, M. D., Dubal, H.-R., Butler, L. J. & Crim, F. F. 1987 *J. chem. Phys.* **87**, 5820–5829.

Vander Wal, R. L. & Crim, F. F. 1989 *J. phys. Chem.* **93**, 5331–5333.

Vasudev, R., Zare, R. N. & Dixon, R. N. 1984 *J. chem. Phys.* **80**, 4863–4878.

Weide, K., Kuhl, K. & Schinke, R. 1989 *J. chem. Phys.* **91**, 3999–4008.

Zare, R. N. 1982 *Ber. BunsenGes. phys. Chem.* **86**, 422–425.

Zewail, A. H. 1989 *J. chem. Soc. Faraday Trans.* II **85**, 1221–1242.

Discussion

F. F. Crim (*University of Wisconsin, U.S.A.*). E. L. Sibert has calculated the nature of the molecular eigenstates in HOOH to assess the extent of O–O stretching state admixture. He finds a large number of zero-order states in the molecular eigenstate but none makes a dominant contribution except for the O–H stretching states. There are, however, a number of states with significant amounts of O–O stretching excitation. It appears that these minor components are the key to efficient vibrationally mediated photodissociation. The O–O stretching excitation makes the photodissociation very efficient.

J. P. Simons. The weak contamination of the O–H local mode by admixtures of O–O stretching modes is, of course, crucially important in promoting the vibrationally mediated photodissociation of HOOH into two OH fragments. It is this pathway that 'picks out' the minor components in the vibrational eigenfunction. Future two-colour experiments at total absorbed energies in excess of the H–OOH bond dissociation energy may allow estimates of the $(H + HO_2)/(OH + OH)$ branching ratios.

PHILOSOPHICAL TRANSACTIONS OF THE ROYAL SOCIETY A MATHEMATICAL, PHYSICAL & ENGINEERING SCIENCES